Sol–Gel Synthesis of Cerium-Doped Tio_2 Nanoparticles with Enhanced Visible-Light Absorption as Candidate Electron Transport Materials for Perovskite Solar Cells

K. Jhansi Rani[1*], C. V. Krishna Reddy[2]

[1]Research Scholar, Department of Physics, Rayalaseema University, Kurnool 518007, Andhra Pradesh, India

[2]Professor, Department of Physics, Rayalaseema University, Kurnool 518007, Andhra Pradesh, India

***Corresponding Author**

DOI: https://doi.org/10.51584/IJRIAS.2026.11100117

Received: 31 October 2026; Accepted: 05 November 2026; Published: 19 November 2026

ABSTRACT

Titanium dioxide is the most widely used electron transport layer (ETL) in n–i–p perovskite solar cells (PSCs), but its wide band gap, modest electron mobility and high density of recombination-active defects limit device performance. In this work, pure and cerium-doped TiO_2 (Ce:TiO_2) nanoparticles with nominal Ce contents of 1.2, 1.5, 1.8, 2.1 and 2.4 mol% were prepared by an acetic-acid-modified sol–gel route followed by calcination at 450 °C, and their structural, morphological and optical properties were characterised as a materials-level assessment; no solar-cell devices were fabricated. X-ray diffraction showed that all samples crystallised as single-phase anatase (JCPDS 21-1272) with no detectable CeO_2 or $Ce_2Ti_2O_7$ reflections, while peak broadening indicated a decrease in the Scherrer crystallite size from 11.1 nm (pure TiO_2) to 5.5–7.4 nm in the doped samples (estimated uncertainty ≤ ±0.3 nm from the diffractometer step size; values are lower-bound estimates). Scanning electron microscopy showed agglomerates of approximately 130–350 nm built from finer primary crystallites, and FTIR spectra confirmed the Ti–O–Ti lattice framework and indicated increased surface hydroxylation upon doping. Pure TiO_2 showed an indirect optical band gap of 3.31 eV. Ce incorporation increased sub-band-gap absorption across the visible region, raising the absorbance at 500 nm from 0.12 to 0.46–2.63 with increasing Ce content. Because this absorption masks the fundamental absorption edge, the band gap of the doped samples could not be determined, and the enhanced absorption is attributed to Ce 4f- and defect-related states rather than to band-gap narrowing. The reduced crystallite size and the dopant-related sub-gap states indicate that low-level Ce doping is a simple, solution-processable route for modifying TiO_2; whether these changes improve electron transport or photovoltaic performance remains to be established in device studies.

Keywords: Cerium-doped TiO_2; sol–gel synthesis; anatase; crystallite size; visible-light absorption; electron transport layer; perovskite solar cells

INTRODUCTION

Organic–inorganic halide perovskite solar cells (PSCs) have advanced faster than any other photovoltaic technology since metal halide perovskites were first used as light absorbers in 2009 [1]. Much of this progress has come from mesoscopic and planar n–i–p architectures in which a thin perovskite absorber is sandwiched between an electron transport layer (ETL) and a hole transport layer [2,3]. The ETL must extract photogenerated electrons, block holes, and provide a chemically stable interface with the perovskite, so its optical, electronic and morphological properties directly govern the short-circuit current density (J_{sc}), open-circuit voltage (V_{oc}) and fill factor (FF) of the device.

Titanium dioxide (TiO_2) remains the benchmark ETL owing to its favourable conduction-band alignment with common perovskites, chemical stability, non-toxicity and low cost [4–6]. Its versatility is reflected in a broad range of established applications, including photocatalysis [6,7], humidity and gas sensing [8,9], filtration

ISSN No. 2454-6194 | DOI: 10.51584/IJRIAS |Volume XI Issue X October 2026

membranes [10], dye-sensitised solar cells [11], optical encapsulants [12] and photonic crystals [13]. However, pristine anatase TiO_2 has a wide band gap (≈3.2 eV), relatively low electron mobility and a high density of sub-gap trap states, which together promote interfacial charge recombination and limit the performance of TiO_2-based PSCs [14].

Doping with rare-earth elements is an effective way to tailor these properties. Cerium is particularly attractive because the facile Ce^{3+}/Ce^{4+} redox couple promotes the formation of oxygen vacancies, introduces localised Ce 4f states below the TiO_2 conduction band that can act as shallow electron traps, and retards grain growth during calcination [15–17]. Ce doping of mesoporous TiO_2 has been shown to modify crystal growth and the flat-band potential and to raise PSC efficiency [14], and cerium oxide itself has been demonstrated as a low-temperature ETL [15]. Nevertheless, systematic studies that correlate Ce content in sol–gel-derived TiO_2 nanoparticles with structure, crystallite size, surface chemistry and optical absorption remain limited.

In this work, we prepare a series of Ce:TiO_2 nanoparticles (0–2.4 mol% Ce) by a controlled, acetic-acid-chelated sol–gel route and characterise them by XRD, SEM, FTIR and UV–Vis absorption spectroscopy. The study is a materials-level assessment: we relate the dopant-induced changes in crystal structure, crystallite size, surface chemistry and optical absorption to the properties expected to matter for an ETL in n–i–p PSCs. Solar-cell devices were not fabricated, so the work does not claim improvements in electron transport, charge extraction or photovoltaic efficiency; these are identified as hypotheses for future device-level investigation.

EXPERIMENTAL

2.1 Materials

Titanium(IV) isopropoxide (TTIP, 97%, Sigma-Aldrich), cerium(III) nitrate hexahydrate ($Ce(NO_3)_3 \cdot 6H_2O$, ≥99%, Sigma-Aldrich, absolute ethanol (≥99.8%, Merck) and glacial acetic acid (≥99.5%, Sigma-Aldrich) were used as received without further purification. Distilled water was used throughout.

2.2 Synthesis of pure and Ce-doped TiO_2 nanoparticles

Ce:TiO_2 nanoparticles with nominal Ce/(Ce + Ti) ratios of 0, 1.2, 1.5, 1.8, 2.1 and 2.4 mol% were prepared by a sol–gel process. In a typical synthesis, 10 mL of TTIP was added to 50 mL of absolute ethanol under continuous magnetic stirring at room temperature, and 5 mL of glacial acetic acid was then added as a chelating agent to moderate the hydrolysis rate. Separately, the required amount of $Ce(NO_3)_3 \cdot 6H_2O$ was dissolved in a 1:1 (v/v) water–ethanol mixture and added dropwise to the titanium sol. Distilled water was then introduced slowly to give a H_2O:TTIP molar ratio of approximately 4:1, while the pH was held at 2–3 with acetic acid to prevent uncontrolled precipitation. The resulting sol was stirred for 3 h and aged for 24 h at room temperature to form a gel. The gel was dried at 100 °C for 12 h to obtain a xerogel, which was ground and calcined in air at 450 °C for 3 h at a heating rate of 3 °C min^{-1}. Pure TiO_2 was prepared by the same procedure without the cerium precursor.

2.3 Characterisation

Powder X-ray diffraction (XRD) patterns were recorded on a Rigaku Ultima IV diffractometer using Cu Kα radiation (λ = 1.5406 Å) over 2θ = 10–70° at a step size of 0.02°. The average crystallite size (D) was estimated from the anatase (101) reflection using the Scherrer equation:

$$D = K\lambda / (\beta \cos \theta) \qquad (1)$$

where $K = 0.9$ is the shape factor, β is the measured full width at half maximum (in radians) and θ is the Bragg angle. Because β was not corrected for instrumental broadening, the calculated values of D are lower-bound estimates. Morphology was examined with a scanning electron microscope (Carl Zeiss, EVO MA10) operated at 5–10 kV. FTIR spectra were collected in the range 4000–400 cm^{-1} on a Thermo Scientific Nicolet iS50 spectrometer using the KBr pellet method. UV–Vis absorption spectra were recorded from 200 to 800 nm on a Shimadzu UV-2600i spectrophotometer. The optical band gap (E_g) was determined from Tauc plots assuming an indirect allowed transition for anatase:

$$(\alpha h\nu)^{1/2} = A\,(h\nu - E_g) \qquad (2)$$

where α is the absorption coefficient, $h\nu$ the photon energy and A a constant.

2.4 Replication and measurement uncertainty

Each composition was prepared as a single synthesis batch and each characterisation was performed once on that batch, so the values reported are single measurements and batch-to-batch statistics are not available. Measurement uncertainties were therefore estimated from instrumental resolution. For XRD, peak positions and FWHM values are taken to be uncertain by ±0.02° (one step), which propagates to an uncertainty in D of about ±0.3 nm for pure TiO_2 and ±0.1 nm for the doped samples. This random uncertainty is smaller than the systematic uncertainty of the Scherrer method itself (choice of K, neglect of instrumental and strain broadening), which is typically 10–20%; crystallite sizes should therefore be compared as trends rather than as absolute values. SEM agglomerate sizes are the ranges observed across the imaged fields rather than statistical size distributions. UV–Vis absorbance values are quoted to two decimal places; the differences between samples at 500 nm (0.12–2.63) are much larger than the photometric repeatability of the instrument.

RESULTS AND DISCUSSION

3.1 Structural analysis

Fig. 1 shows the XRD patterns of pure and Ce-doped TiO_2. All samples display the characteristic reflections of tetragonal anatase TiO_2 (JCPDS No. 21-1272), indexed to the (101), (004), (200), (105)/(211) and (204) planes at $2\theta \approx 25.3°$, 37.8°, 48.0°, 53.9°/55.1° and 62.7°, respectively. No reflections attributable to rutile, CeO_2 or other cerium-containing phases are detected at any doping level, indicating that cerium is either incorporated into the anatase lattice or highly dispersed below the detection limit of XRD.

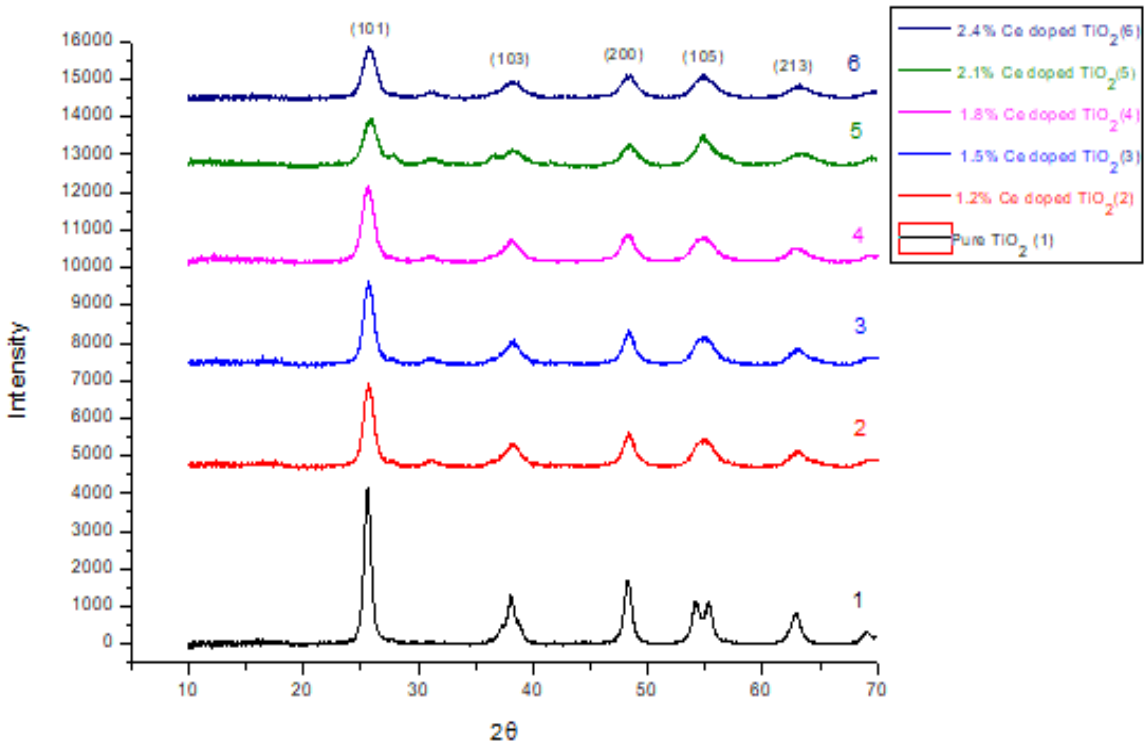


Fig. 1. XRD patterns of (1) pure TiO_2 and (2–6) Ce:TiO_2 nanoparticles containing 1.2, 1.5, 1.8, 2.1 and 2.4 mol% Ce, calcined at 450 °C. All reflections match anatase TiO_2 (JCPDS No. 21-1272).

Compared with pure TiO_2, the doped samples exhibit markedly broader and less intense reflections; the (105) and (211) peaks merge into a single broad feature, and the FWHM of the (101) reflection increases from 0.73° for pure TiO_2 to 1.10–1.47° for the doped samples. The crystallite size calculated from Eq. (1) decreases from

11.1 nm for pure TiO_2 to 7.4 nm at 1.2–1.5 mol% Ce and reaches a minimum of 5.5 nm at 2.1 mol% Ce, with a slight recovery to 6.3 nm at 2.4 mol% (Table 1). For most doped samples the (101) reflection shifts slightly to higher angle, from 25.55° to 25.64–25.83°, while the 1.8 mol% sample remains at 25.55°. Because these shifts are small (0.09–0.28°, i.e. 5–14 diffractometer steps) and do not vary monotonically with Ce content, they are interpreted cautiously as a small contraction of the interplanar spacing (d_{101} = 3.483 Å for pure TiO_2) and lattice strain upon doping. Because the ionic radii of Ce^{4+} (0.87 Å) and Ce^{3+} (1.01 Å) are considerably larger than that of Ti^{4+} (0.605 Å) in six-fold coordination [18], only limited substitution is expected, and the absence of lattice expansion suggests that most Ce does not occupy substitutional Ti sites but is located at crystallite surfaces and grain boundaries, possibly as Ti–O–Ce linkages, where it can hinder the diffusion and growth of TiO_2 grains during calcination. Such growth inhibition by Ce is consistent with previous reports [14,16]. The cerium location and oxidation state were not determined directly in this work.

Table 1. Structural parameters (anatase (101) reflection) of pure and Ce-doped TiO_2 nanoparticles obtained from XRD.

Sample	(101) position, 2θ (°)	FWHM, β (°)	Crystallite size, D (nm)
Pure TiO_2	25.55	0.73	11.1
1.2 mol% Ce:TiO_2	25.64	1.10	7.4
1.5 mol% Ce:TiO_2	25.64	1.10	7.4
1.8 mol% Ce:TiO_2	25.55	1.27	6.4
2.1 mol% Ce:TiO_2	25.83	1.47	5.5
2.4 mol% Ce:TiO_2	25.74	1.29	6.3

D calculated with K = 0.9 and λ = 1.5406 Å, without instrumental-broadening correction. Estimated uncertainties: 2θ and FWHM ±0.02° (one diffractometer step); D ±0.3 nm (pure TiO_2) and ±0.1 nm (doped samples). Single measurement per composition.

3.2 Morphology

Representative SEM images of the Ce:TiO_2 powders are shown in Fig. 2. The samples consist of irregular, quasi-spherical agglomerates with measured dimensions of approximately 130–350 nm. These agglomerates are much larger than the crystallite sizes obtained from XRD, indicating that each is composed of many primary nanocrystallites that cluster during gelation and calcination, as is typical of sol–gel-derived oxide powders. With increasing Ce content the agglomerates become smaller and more uniform, in agreement with the dopant-induced grain-growth inhibition inferred from XRD.

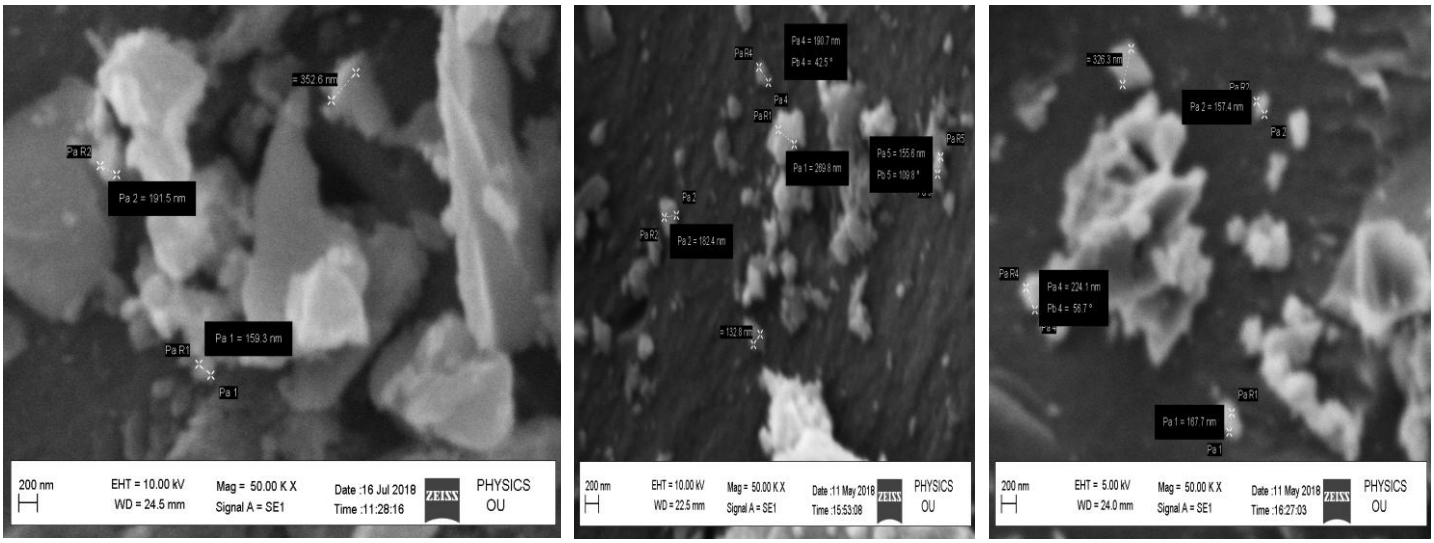


Fig. 2. SEM images (50 000×) of Ce:TiO_2 nanoparticles: (a) pure, (b)1.5 mol% Ce and (c)2.1 mol% Ce. Scale bar: 200 nm.

ISSN No. 2454-6194 | DOI: 10.51584/IJRIAS |Volume XI Issue X October 2026

3.3 FTIR analysis

FTIR spectra of pure TiO_2 and Ce:TiO_2 containing 1.2, 1.5 and 1.8 mol% Ce are shown in Fig. 3. The broad, intense absorption below ≈800 cm^{-1} arises from Ti–O and Ti–O–Ti stretching vibrations of the anatase framework. The broad band centred near 3400 cm^{-1} and the weaker band near 1630 cm^{-1} are assigned to the O–H stretching and H–O–H bending modes of surface hydroxyl groups and adsorbed water, respectively, while the weak feature near 2350 cm^{-1} is due to atmospheric CO_2. Upon Ce doping, the Ti–O–Ti band shifts slightly to 550-650 cm^{-1}, consistent with lattice distortion caused by Ce incorporation, and the hydroxyl-related bands become relatively stronger. The enhanced surface hydroxylation may reflect a higher density of surface defect sites, such as oxygen vacancies, that act as adsorption sites for water; however, oxygen vacancies were not quantified directly in this work. No distinct Ce–O vibration of a segregated CeO_2 phase is resolved, in agreement with the XRD results.

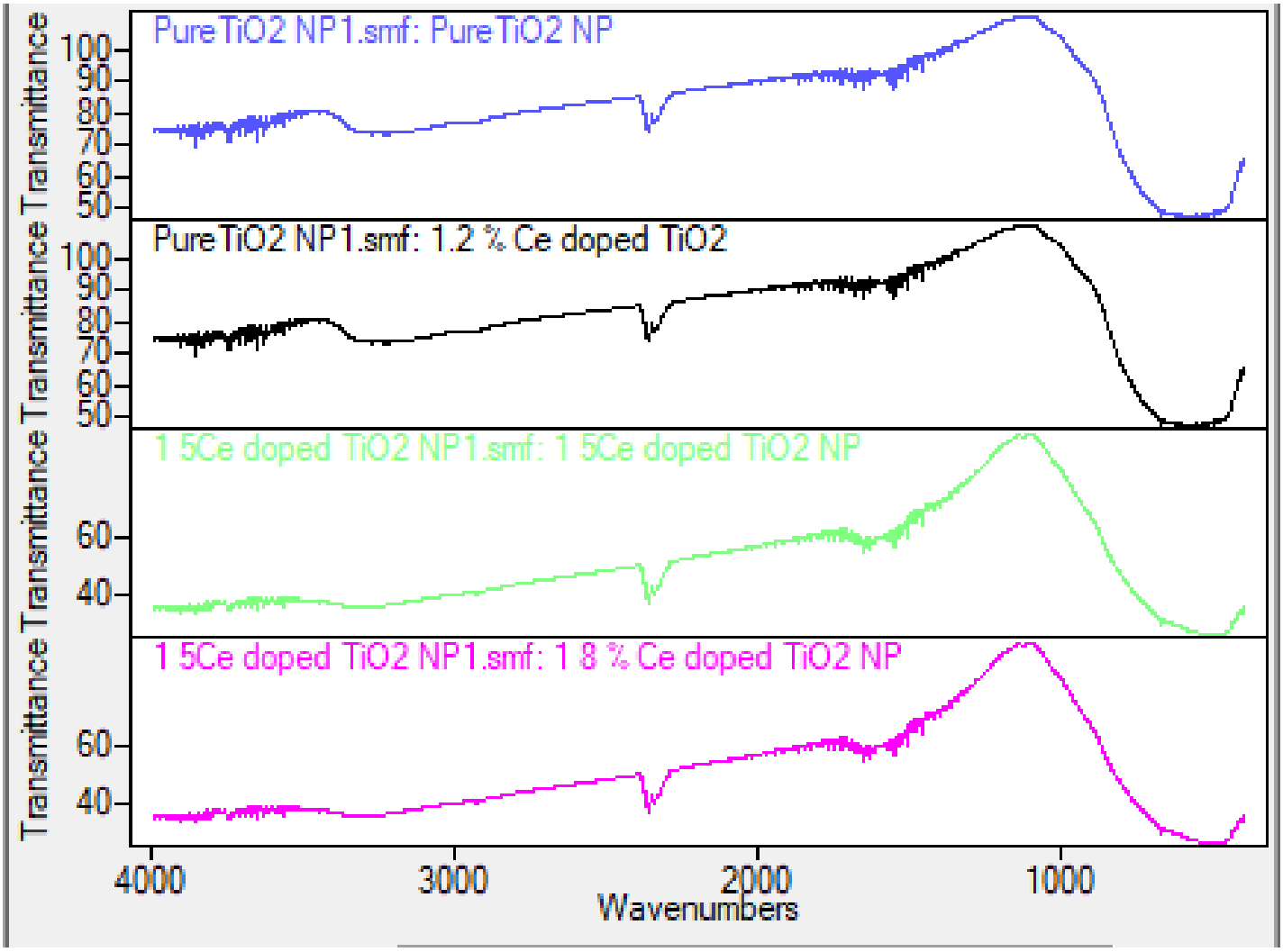


Fig. 3. FTIR spectra of pure TiO_2 and Ce:TiO_2 nanoparticles containing 1.2, 1.5 and 1.8 mol% Ce.

3.4 Optical properties

The UV–Vis absorption spectra are presented in Fig. 4. Pure TiO_2 shows the strong band-edge absorption of anatase in the UV region, with negligible absorption above ≈400 nm. Ce incorporation increases the absorption across the entire 400–800 nm range, and this sub-band-gap absorption grows systematically with Ce content, being most pronounced for the 2.1 and 2.4 mol% samples. The minor discontinuity near 280 nm in all spectra arises from the lamp changeover of the spectrophotometer and is not a sample feature. Based on previous reports, the enhanced visible absorption is attributed to O 2p → Ce 4f charge-transfer transitions, Ce^{3+}/Ce^{4+} intervalence transitions, and absorption by defect states, such as oxygen vacancies, within the band gap [16,17].

ISSN No. 2454-6194 | DOI: 10.51584/IJRIAS |Volume XI Issue X October 2026

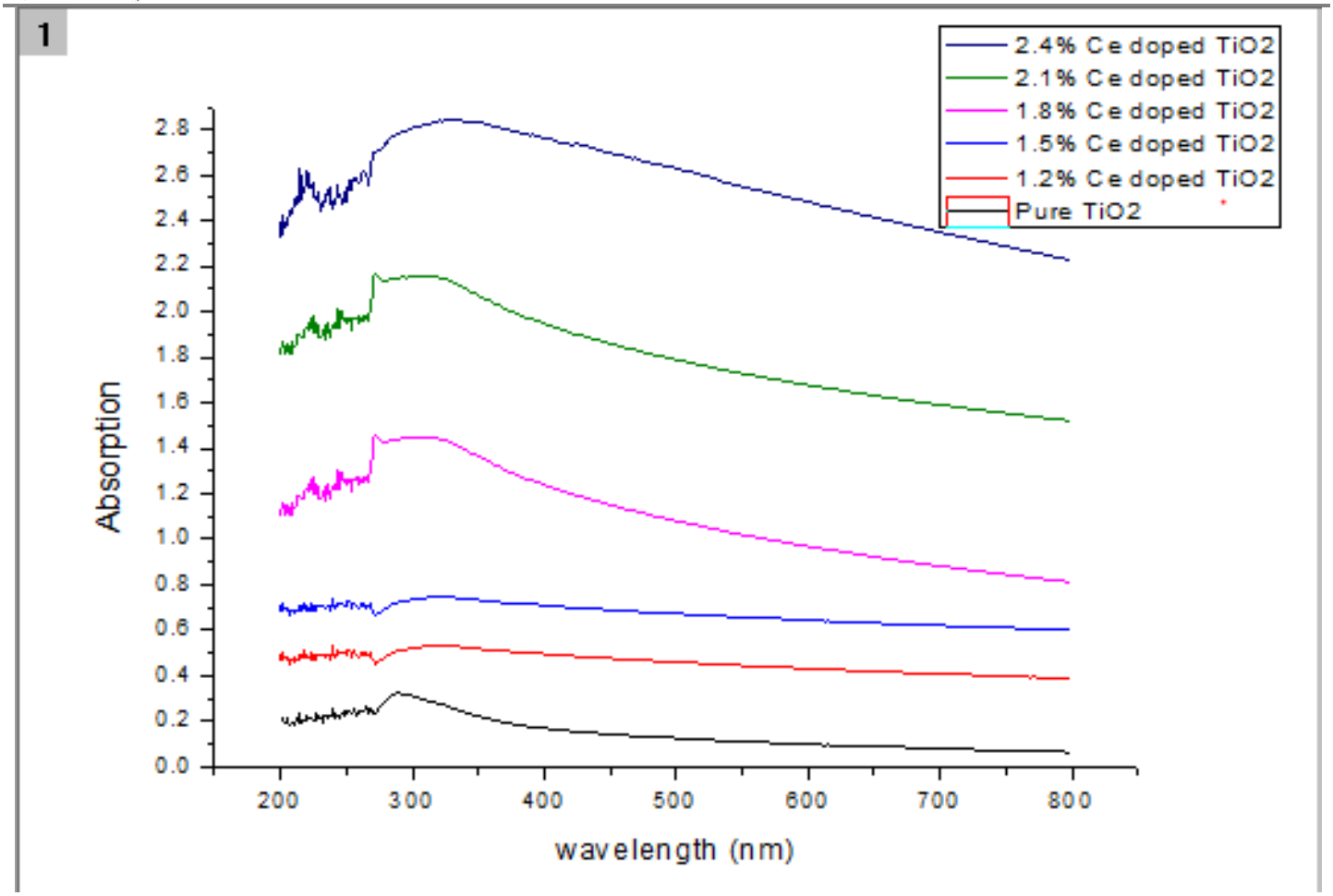


Fig. 4. UV–Vis absorption spectra of pure TiO_2 and Ce:TiO_2 nanoparticles containing 1.2–2.4 mol% Ce. Spectra are as measured; the step near 280 nm is an instrumental artefact.

The Tauc plot of pure TiO_2 (Eq. 2; Fig 4) yields an indirect band gap of 3.31 eV (absorption edge ≈375 nm), in good agreement with the reported value for anatase [4]. For the Ce-doped samples, the strong sub-band-gap absorption extending to 800 nm masks the fundamental edge, so a reliable linear Tauc region could not be identified from the absorbance spectra. The effect of doping is therefore quantified in Table 2 through the absorbance at 500 nm, which rises from 0.12 for pure TiO_2 to 0.46, 0.68, 1.08, 1.78 and 2.63 for 1.2, 1.5, 1.8, 2.1 and 2.4 mol% Ce, respectively; even when normalised to the UV maximum, the visible absorbance increases from 38% to 74–92%. This increase reflects additional sub-gap absorption and is not evidence of band-gap narrowing: the present data neither establish nor exclude a shift of the fundamental edge. Determining this would require diffuse-reflectance measurements with Kubelka–Munk analysis or transmission measurements on thin films. For PSC applications, dopant-related states below the conduction band may modify electron transfer at the TiO_2/perovskite interface, but this was not tested here.

Table 2. Optical parameters of pure and Ce-doped TiO_2 obtained from UV–Vis absorption spectra.

Sample	**λ_{max} (nm)**	**A at λ_{max}**	**A at 500 nm**	**A_{500}/A_{max} (%)**	**E_g (eV)**
Pure TiO_2	290	0.33	0.12	38	3.31
1.2 mol% Ce:TiO_2	335	0.53	0.46	87	n.r.
1.5 mol% Ce:TiO_2	332	0.75	0.68	90	n.r.
1.8 mol% Ce:TiO_2	317	1.45	1.08	74	n.r.
2.1 mol% Ce:TiO_2	317	2.15	1.78	83	n.r.
2.4 mol% Ce:TiO_2	335	2.84	2.63	92	n.r.

n.r. = not resolved: the band edge is masked by sub-gap absorption in the absorbance spectra.

3.5 Implications and limitations for ETL application

The present results characterise Ce:TiO_2 as a material and do not include device fabrication, so their relevance to PSCs is indicative only. Three limitations should be noted. First, electron transport, charge extraction and photovoltaic performance were not measured. Claims in these areas require n–i–p devices with Ce:TiO_2 ETLs, characterised by current density–voltage measurements, external quantum efficiency and impedance spectroscopy.

Second, charge-carrier dynamics were not studied, so the present data do not show whether Ce doping improves charge separation or suppresses recombination. Addressing this would require transient measurements on perovskite/ETL bilayers, conductivity or electron-mobility measurements, and band-alignment measurements (for example, ultraviolet photoelectron spectroscopy or Mott–Schottky analysis).

Third, the strong visible absorption of the more heavily doped samples could be a drawback for an ETL in n–i–p devices, where light passes through the ETL before reaching the perovskite; parasitic absorption in the ETL could reduce the photocurrent. In thin compact or mesoporous films this loss may be small, but it should be quantified. On this basis, the lower Ce contents (1.2–1.5 mol%), which combine a reduced crystallite size with comparatively weak visible absorption, appear the most suitable for future device testing.

CONCLUSIONS

Pure and Ce-doped TiO_2 nanoparticles (1.2–2.4 mol% Ce) were synthesised by an acetic-acid-chelated sol–gel route and calcined at 450 °C. All samples retained the single-phase anatase structure, and Ce incorporation inhibited grain growth, reducing the Scherrer crystallite size from 11.1 nm to a minimum of 5.5 nm at 2.1 mol% Ce. FTIR indicated increased surface hydroxylation upon doping. Pure TiO_2 showed a band gap of 3.31 eV, and Ce doping extended optical absorption across the visible region (absorbance at 500 nm increasing up to 22-fold); because this sub-gap absorption masked the fundamental edge, the band gap of the doped samples could not be determined and band-gap narrowing is not claimed. These structural and optical changes make Ce:TiO_2 a candidate electron transport material for perovskite solar cells. However, no devices were fabricated in this study, so its effect on electron transport, charge extraction and photovoltaic efficiency remains to be demonstrated. Future work will focus on fabricating n–i–p devices with Ce:TiO_2 ETLs; measuring charge-carrier dynamics in perovskite/ETL bilayers; determining the conduction-band position, the location and oxidation state of Ce and electron mobility as functions of Ce content; quantifying parasitic absorption in the ETL; and evaluating long-term operational stability.

REFERENCES

1. A. Kojima, K. Teshima, Y. Shirai, T. Miyasaka, Organometal halide perovskites as visible-light sensitizers for photovoltaic cells, J. Am. Chem. Soc. 131 (2009) 6050–6051. https://doi.org/10.1021/ja809598r
2. M. M. Lee, J. Teuscher, T. Miyasaka, T. N. Murakami, H. J. Snaith, Efficient hybrid solar cells based on meso-superstructured organometal halide perovskites, Science 338 (2012) 643–647.
3. J. Burschka, N. Pellet, S.-J. Moon, R. Humphry-Baker, P. Gao, M. K. Nazeeruddin, M. Grätzel, Sequential deposition as a route to high-performance perovskite-sensitized solar cells, Nature 499 (2013) 316–319.
4. X. Chen, S. S. Mao, Titanium dioxide nanomaterials: synthesis, properties, modifications, and applications, Chem. Rev. 107 (2007) 2891–2959.
5. U. Diebold, The surface science of titanium dioxide, Surf. Sci. Rep. 48 (2003) 53–229.
6. K. Hashimoto, H. Irie, A. Fujishima, TiO2 photocatalysis: a historical overview and future prospects, Jpn. J. Appl. Phys. 44 (2005) 8269–8285.
7. D. S. Kim, S.-Y. Kwak, The hydrothermal synthesis of mesoporous TiO2 with high crystallinity, thermal stability, large surface area, and enhanced photocatalytic activity, Appl. Catal. A: Gen. 323 (2007) 110–118.
8. P.-G. Su, Y.-P. Chang, Low-humidity sensor based on a quartz-crystal microbalance coated with polypyrrole/Ag/TiO2 nanoparticles composite thin films, Sens. Actuators B 129 (2008) 915–920.

9. G. Sarala Devi, T. Hyodo, Y. Shimizu, M. Egashira, Synthesis of mesoporous TiO2-based powders and their gas-sensing properties, Sens. Actuators B 87 (2002) 122–129.
10. A. Sotto, A. Boromand, S. Balta, S. Darvishmanash, J. Kim, B. Van der Bruggen, Nanofiltration membranes enhanced with TiO2 nanoparticles: a comprehensive study, Desalin. Water Treat. 34 (2011) 179–183.
11. X. Xin, M. Scheiner, M. Ye, Z. Lin, Surface-treated TiO2 nanoparticles for dye-sensitized solar cells with remarkably enhanced performance, Langmuir 27 (2011) 14594–14598.
12. F. W. Mont, J. K. Kim, M. F. Schubert, E. F. Schubert, R. W. Siegel, High-refractive-index TiO2-nanoparticle-loaded encapsulants for light-emitting diodes, J. Appl. Phys. 103 (2008) 083120.
13. J. E. G. J. Wijnhoven, W. L. Vos, Preparation of photonic crystals made of air spheres in titania, Science 281 (1998) 802–804.
14. H. Lu, J. Zhuang, Z. Ma, W. Zhou, H. Xia, Z. Xiao, H. Zhang, H. Li, Crystal recombination control by using Ce doped in mesoporous TiO2 for efficient perovskite solar cells, RSC Adv. 9 (2019) 1075–1083. https://doi.org/10.1039/C8RA07800A
15. X. Wang, L. Deng, L. Wang, S. Dai, Z. Xing, X. Zhan, X. Lu, S. Xie, R. Huang, L. Zheng, Cerium oxide standing out as an electron transport layer for efficient and stable perovskite solar cells processed at low temperature, J. Mater. Chem. A 5 (2017) 1706–1712. https://doi.org/10.1039/C6TA07541J
16. M.-H. Tong et al., Cerium synchronous doping in anatase for enhanced photocatalytic hydrogen production from ethanol–water mixtures, Molecules 28 (2023) 2433. https://doi.org/10.3390/molecules28062433
17. L. Jing, X. Sun, W. Cai, X. Li, H. Fu, H. Hou, N. Fan, Photoluminescence of Ce doped TiO2 nanoparticles and their photocatalytic activity, Acta Chim. Sin. 61 (2003) 1241–1245.
18. R. D. Shannon, Revised effective ionic radii and systematic studies of interatomic distances in halides and chalcogenides, Acta Crystallogr. A 32 (1976) 751–767.